Available at www.sciencedirect.com

SciVerse ScienceDirect

journal homepage: www.elsevier.com/locate/carbon

The chemical and structural analysis of graphene oxide with different degrees of oxidation

Karthikeyan Krishnamoorthy [a], *Murugan Veerapandian* [b], *Kyusik Yun* [b], *S.-J. Kim* [a,c,*]

[a] *Nanomaterials and System Lab., Department of Mechanical System Engineering, Jeju National University, Jeju 690-756, South Korea*
[b] *Department of Bionanotechnology, Gachon University, Gyeonggi-do 461-701, South Korea*
[c] *Department of Mechatronics Engineering, Jeju National University, Jeju 690-756, South Korea*

ARTICLE INFO

Article history:
Received 7 August 2012
Accepted 10 October 2012
Available online 22 October 2012

ABSTRACT

Graphene oxide (GO) with various degrees of oxidation was synthesized using a modified Hummers method. The formation of different types of oxygen containing functional groups in GO, and their influences on its structure were analyzed using X-ray diffraction (XRD), Fourier transform infra-red spectra, X-ray photoelectron spectra (XPS), zeta potential analysis and Raman spectroscopy. XRD studies showed a disruption of the graphitic *AB* stacking order during the increase in oxidation levels. XPS analysis revealed the formation of hydroxyl and carboxyl groups at lower oxidation levels and epoxide groups at higher oxidation levels. The influence of the oxidation degree on the properties of GO was evaluated by zeta potential analysis, which showed a linear increase in the zeta potential with increasing oxidation levels. Raman spectroscopy analysis revealed that increasing oxidation levels results in a transition from a crystalline to an amorphous structure. The electrochemical properties of GO is highly influenced by the variation in degree of oxidation. Our results suggest that the properties of GO can be tuned by varying the oxidation degree, which may pave the way to new developments in the GO-based applications.

1. Introduction

Graphene oxide (GO) is an atomic sheet of graphite decorated by several oxygenated functional groups on its basal planes and at its edges, resulting in a hybrid structure comprising a mixture of sp^2 and sp^3 hybridized carbon atoms [1]. GO can be synthesized by the oxidation of graphite into graphite oxide followed by the exfoliation of this graphitic oxide into GO [2]. It is already well known that chemically both graphite oxide and GO have similar or identical structures. Both possess stacked structures with chemical functionality on their basal planes and at their edges [3]. The only difference between them is the number of stacked layers, GO possess a monolayer or just a few stacked layers, while graphite oxide contains a greater number of stacked layers [3,4]. The formation of oxygenated functional groups in graphite oxide makes them easier to exfoliate into monolayers of GO by simple stirring or mild sonication [5]. Even though, this material has been well known since 1859 when it was first synthesized by Brodie [6], the material only becomes of widespread interest after the discovery of graphene and is due to the fact it acts as a major precursor for the synthesis of graphene sheets by suitable reduction techniques either chemically or thermally [7].

Apart from the synthesis of graphene, GO has several standalone applications in various fields such as optoelectronics, supercapacitors, memory devices, composite materials, photocatalysis and as a drug delivery agent [8–11]. This has drawn the attention of researchers to explore the intriguing properties of GO nanosheets. Most of the outstanding

* *Corresponding author:* Fax: +82 64 756 3886.
E-mail address: kimsangj@jejunu.ac.kr (S.-J. Kim).
0008-6223/$ - see front matter
http://dx.doi.org/10.1016/j.carbon.2012.10.013

properties of GO arise from its hybrid electronic structure as it contains both the conducting π states from the sp^2 carbon domains and also the σ states from the sp^3 carbon domains [12]. Theoretical studies have revealed that the properties of GO can be altered by tuning the sp^2/sp^3 ratios of the carbon atoms [13]. Previous experimental reports showed the observation of quantum confinement phenomena in GO due to the formation of unoxidized sp^2 islands between the oxidized sp^3 regions [14]. The formation of sp^3 domains in GO is due to the oxidation reaction which results in the decoration of different types of functional groups such as hydroxyl, epoxyl, carbonyl and carboxyl groups. The presence of these oxygenated functional groups in GO makes it hydrophilic in nature and also enables them to functionalize other materials with suitable chemistry [15].

The sp^2/sp^3 ratios in GO can be tuned by varying the oxidation degree using suitable chemical reactions. GO with various ratio of sp^2/sp^3 domains may provide novel properties that can be useful for making several improvements in the development of graphene based research applications such as biosensors, supercapacitors, and optoelectronic devices etc., With the motivation of altering the properties of GO by varying the oxidation levels, we used a modified Hummers method employing various quantities of oxidizing agent. To date, three major methods have been used to synthesize GO viz. (i) the Brodie method [6], (ii) the Staudenmaier method [16], and (iii) the Hummers method [17]. Of these methods, the Hummers method is generally considered to be the best and most researchers follow it since it has the advantage of non-toxicity compared to the former two which involve highly toxic reactions due to the liberation of toxic gases and highly reactive species [3]. In this paper, we report on the synthesis of GO with different oxidation levels and investigated their chemical and structural analysis using X-ray diffraction (XRD), Fourier transform infra red spectra (FTIR), X-ray photoelectron (XPS) analysis, zeta potential, transmission electron microscopy (TEM) and Raman spectroscopy. The degree of oxidation is also studied by analyzing their electrochemical properties.

2. Experimental

2.1. Materials

Graphite powder with a size less than 20 μm was purchased from Sigma–Aldrich, USA. Sulphuric acid, potassium permanganate, hydrochloric acid and hydrogen peroxide were purchased from Daejung Chemicals and Metal Ltd., South Korea. All the chemicals obtained were research grade. Doubly distilled water was used throughout the experiment. The ultrasound irradiation was carried out on a SONIC VCX 750 model (20 kHz, 750 W) using a direct immersion titanium horn.

2.2. Synthesis of GO with different degrees of oxidation

GO was synthesized using the harsh oxidation of graphite according to the modified Hummers method by employing $KMnO_4$ and conc. H_2SO_4, followed by ultrasonication [9]. Briefly, graphite powders (2 g) were stirred in 98% H_2SO_4 (45 mL) for 2 h. The required amount of $KMnO_4$ was gradually added to the above solution while keeping the temperature at less than 20 °C. The mixture was then stirred at 35 °C for 2 h. The resulting solution was diluted by adding 90 mL of water under vigorous stirring. The suspension was further treated by adding 30% H_2O_2 solution (10 mL) and 150 mL of distilled water. The resulting graphite oxide suspension was washed by repeated centrifugation, first with 5% HCl aqueous solution and then with distilled water until the *p*H of the solution became neutral. The GO nanosheets were obtained by adding 160 mL of water to the resulting graphite oxide precipitate and were subjected to ultrasound irradiation for 1 h with the aid of a probe type sonicator for the exfoliation of the graphitic oxide into a GO monolayer. The amount of oxygenated functional groups in the GO was varied by changing the amount of $KMnO_4$ from 1 to 6 g with an increment of 1 g per oxidation level (The other parameters in the reaction were kept constant).

2.3. Instrumentation

XRD characterization was performed on a X-ray Diffractometer System (D/MAX 2200H, Bede 200, Rigagu Instruments C). The FTIR spectrum (1000–2000 cm^{-1}) was measured using a Thermo scientific FTIR spectrometer with pure KBr as the background. The samples were mixed with KBr and the mixture was dried and compressed into a transparent tablet for measurement. The surface morphology of all the samples was analyzed using a high resolution transmission electron microscope (HR-TEM, FEI Titan 80-300) and a bioatomic force microscope (AFM: Nanowizard II, JPK instruments). The chemical composition and the state of elements present in the outermost parts of the GO nanosheets were investigated by XPS measurements using an ESCA-2000, VG Microtech Ltd. Here a monochromatic X-ray beam source at 1486.6 eV (Aluminum anode) and 14 kV was used to scan the sample surface. A high flux X-ray source with an Aluminum anode was used for X-ray generation, and a quartz crystal monochromator was used to focus and scan the X-ray beam on the sample. The zeta potential measurements of the samples in an aqueous dispersion were performed on Malvern Instruments. The Raman spectra were recorded with a RENISHAW (M005-141) Raman system with laser frequency of 514 nm as an excitation source. The laser spot size was 1 μm and the power at the sample was kept to below 10 mW, in order to avoid laser induced heating. The ultrasound irradiation for the exfoliation of the graphitic oxide into monolayers of GO was carried out on a SONIC VCX 750 model (20 kHz, 750 W) using a direct immersion titanium horn.

The electrochemical properties of all the samples were studied by cyclic voltammetry (CV) measurements using an AUTOLAB PGSTAT320N system with a three-electrode configuration containing a glassy carbon electrode (GCE) as the working electrode, and platinum and an Ag/AgCl electrode as the counter and reference electrodes, respectively. Prior to GO casting, the GCE electrode, was polished with alumina powders, then rinsed thoroughly, and finally blow dried with N_2. A 5 μL suspension of GO samples was spread on the pretreated bare GCE using a micropipette and the film was

allowed to dry in a vacuum desiccator. All the electrochemical measurements were recorded in a 5 mM $K_3[Fe(CN)_6]$ solution containing 0.1 M of KCl solution in the potential range of −0.2 to +0.6 V. A reproducible voltammogram can be obtained under steady-state conditions after about five cycles.

3. Results and discussion

In this study, we used a modified Hummers method to synthesize GO with different degrees of oxidation by adjusting the quantity of oxidizing agent ($KMnO_4$) used in the synthesis reaction. In total, 6 different oxidation levels were synthesized; these were denoted as S-1, S-2, S-3, S-4, S-5 and S-6 where the numbers of the samples indicate the amount (in grams) of $KMnO_4$ used in the oxidation reaction. The photographic images of all samples are presented in Fig. 1. We can observe a change in color from black into blackish brown and finally a brownish yellow color as we move through the samples with different levels of oxygenated functional groups.

3.1. *XRD analysis*

XRD analysis was used to characterize the crystalline nature and phase purity of the as-synthesized GO with different degrees of oxidation. As a reference, the XRD pattern of the pristine graphite is shown in the Supplementary document (Fig. S1). The XRD pattern of the graphite shows a diffraction peak at $2\theta = 26.3°$ corresponding to an interlayer spacing of about 0.34 nm [18]. The XRD patterns of all samples are shown in Fig. 2, these clearly show that with increasing oxidation levels, the intensity of the peak at $2\theta = 26.3°$ starts decreases, and finally, disappears at the higher oxidation levels. Simultaneously, we can also observe the appearance of a new peak at a lower diffraction angle starts to grow with increasing oxidation levels corresponding to the diffraction pattern of GO. The XRD pattern of the synthesized samples shows significant changes in the crystallinity of GO at each stage of oxidation. At upon lower oxidation level of graphite using 1 g of $KMnO_4$, we can see a result in peak broadening around $2\theta = 26.15°$ in the XRD pattern of S-1. The peak broadening effect is due to the lattice distortion that occurs in the *AB* stacking order of the graphite lattice due to mild oxidation.

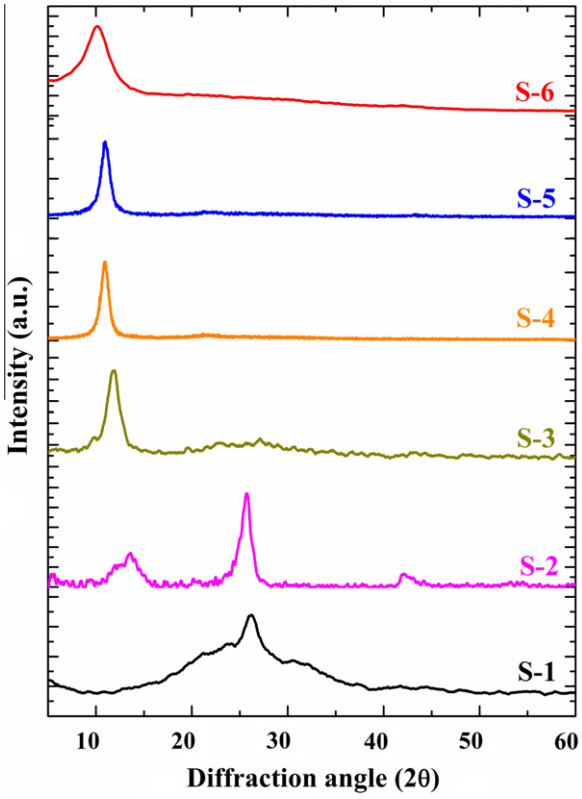

Fig. 2 – X-ray diffraction patterns of GO with different degrees of oxidation.

The peak broadening effect due to mild oxidation of graphite is in good agreement with the experimental results of Jeong et al. [19,20] The increase in oxidation quantity (2 g of $KMnO_4$) results in the following changes as shown in the XRD of sample S-2, viz (i) the graphitic peak at $2\theta = 26.15°$ becomes narrower and (ii) the formation of a new broad peak at $2\theta = 13.3°$ with a lower intensity compared to the graphitic peak. These changes come from the heterogeneous nature of the oxidized graphite comprised of both sp^2 domains from graphite and the sp^3 domains from oxidized graphite. Upto this point, the sample possesses more graphitic domains and less oxidized domains.

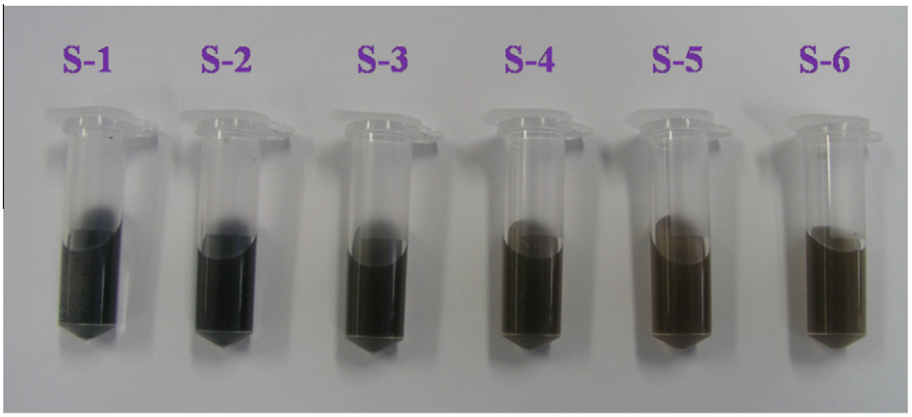

Fig. 1 – Photographic images of GO samples with different degrees of oxidation.

When the concentration of $KMnO_4$ was increased to 3 g, the XRD pattern of S-3 shows that the intensity of the peak at $2\theta = 11.74°$ becomes higher and the peaks due to graphite disappear. The observed interlayer spacing of S-3 was 0.74 which corresponds to the GO. With further increases in the oxidation content, the XRD pattern of samples S-4, S-5, and S-6 contain only the diffraction peaks due to the GO at $2\theta = 10.91°$, 10.52° and 10.12° with an interlayer spacing about 0.81, 0.84, and 0.89 nm, respectively. All together, the XRD analysis revealed that the samples S-1 and S-2 contain more graphitic domains are graphite oxide and the samples S-3, S-4, S-5 and S-6 possess interlayer spacings between 0.74 and 0.89 nm corresponding to the GO. The XRD results of the GO samples are in good agreement with published reports available in the literatures [8,9,18,21]. The increasing interlayer spacing of the GO samples suggests that different levels of oxygen containing groups were attached to the graphite lattice. There were no significant changes occurred in the XRD pattern of GO samples other than the increase in interlayer spacing. This finding is supported by the observations of Lucas et al. [22].

3.2. *Morphological characterization and crystallinity analysis*

The surface morphology and crystalline nature of the synthesized GO with different degrees of oxidation was analyzed using HR-TEM and selected area electron diffraction (SAED) pattern as shown in Fig. 3. It is obvious that all the samples possess a sheet like morphology with different transparencies. This is probably due to the number of layers present in the stacked structure of GO. The HR-TEM results of samples S-1 and S-2 show the sheet like morphology comprised of many layers of partially oxidized graphite oxide. The samples S-1 and S-2 contains less oxygenated functional groups which limits them in terms of exfoliation into monolayers or few layers after the exfoliation process. Also the transparency of these samples is less than the others due to the presence of more layers. However, with increases in the oxidation level, GO samples (S-3, S-4, S-5 and S-6) become highly transparent, since these samples possess high amounts of oxygenated functional groups, which makes suitable for exfoliation into monolayers or just a few layers of GO after ultrasonication. The dimension of the samples is high in the less oxidized samples (S-1 and S-2) and a reduction in sheet length is observed with increasing oxidation level. An overall analysis of the HR-TEM observations shows that the sheets morphology, dimension and the transparency are highly dependent on the level of oxidation and the exfoliation strategy.

The SAED pattern is one of the tools used to characterize the crystalline nature of nanosized materials. The SAED pattern of all the GO samples with different oxidation level is shown in the inset of their corresponding TEM images, as can be seen in Fig. 3. It is observed that the SAED pattern of all the samples possess clear diffraction spots with a six-fold pattern that is consistent with the hexagonal lattice [21].

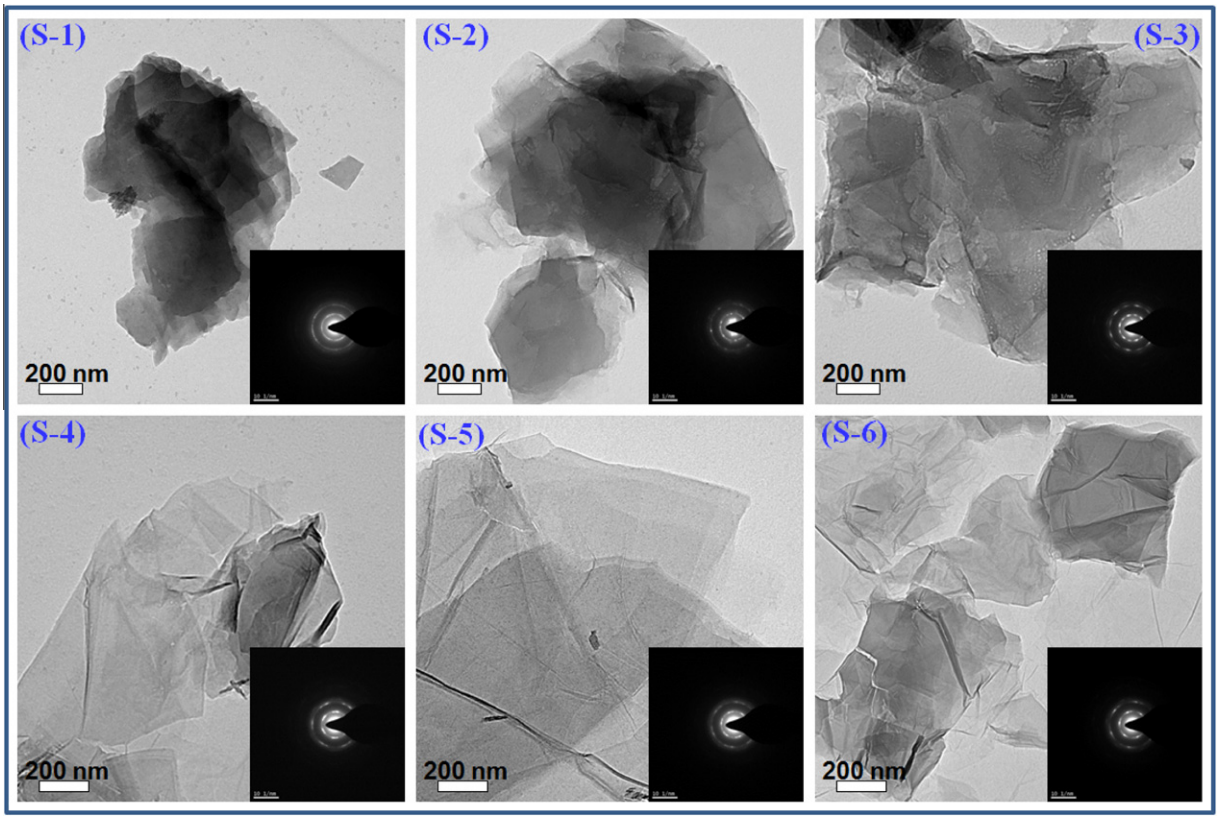

Fig. 3 – High resolution transmission electron microscope images of GO with different degrees of oxidation. The inset in each image shows the SAED pattern of the corresponding sample.

These observations indicate that the graphitic *AB* stacking order is preserved in the lattice even after higher oxidation levels. This is in accordance with the previous studies of Jeong et al. [20], which contains evidence of *AB* stacking order in graphitic oxide produced using Brodie's method. The SAED pattern of the S-1 and S-2 samples shows a typical ring like pattern indicating the polycrystalline nature of the samples. These rings like pattern arise from the merging of the diffraction spots due to the greater number of layers in the samples [23]. This is in accordance with the XRD patterns of the corresponding samples. However an increase in oxidation levels leads to exfoliation into a single or few layered GO resulting in a diffraction pattern due to the superposition of two or three hexagonal pattern of few layered GO. The SAED pattern of the S-6 sample is in accordance with previous studies on the SAED pattern of GO as shown by Wilson et al. [23]. This observed pattern for our sample (S-6) also closely matches graphite oxide samples studied by other groups [24,25]. Similar phenomenon was also observed by Wilson et al. and their work concluded that GO is not only comprised of fully amorphous regions but some crystalline regions are also present [23]. The amorphous region in GO occurred due to the presence of several sp^3 carbon atoms formed during the oxidation reaction. There are a few reports showing the presence of graphitic islands or unoxidized domains (sp^2 content) within the oxidized domains (sp^3 content) in GO [14,26,27]. Our previous study also showed that the presence of graphitic islands in GO results in quantum fluctuations leading to an opening of the band gap in the electronic structure of GO [28]. No diffraction pattern was observed for the oxygenated functional groups in all the samples, rather the hexagonal spots of graphitic nature indicate that the oxygenated functional groups formed on the graphite lattice are not resulted in the formation of any superlattice type ordered arrays [23].

We have also studied the morphology of the GO sample (S-6) using atomic force microscopy. The AFM topography of the GO sample S-6 is shown in Fig 4. It shows a typical sheet like morphology and also resembles the presence of monolayers (Fig 4(d)) and few layered GO (Fig 4(e)). The difference in the number of layers can be easily distinguished using the contrast of the sheets. The monolayers of GO have a light in color whereas the few layered GO are bright in color Fig 4(a). The presence of a few layers in the sample is due to the aggregation or self assembly of two or three layers of GO during the drying process in the specimen preparation. We also examined the nature of monolayer GO, as seen in Fig 4(b) which shows high transparency and some folded regions. Similarly, Fig 4(c) shows the presence of monolayer and few layered GO depicting the presence of wrinkles in the sheets. The AFM studies are in agreement with the TEM observations mentioned above.

3.3. *FT-IR characterization*

In order to study the different types of functional groups formed in the GO at different degrees of functional groups, FT-IR spectroscopy was used. The FT-IR spectra of all samples are shown in Fig. 5. The FT-IR shows band at 1573 cm^{-1} due to the presence of C–C stretching in graphitic domains found in S-1. With further increases in oxidation level, the FT-IR spectrum reveal the presence of C=O (1720 cm^{-1}), C–O (1050 cm^{-1}), C–O–C (1250 cm^{-1}) C–OH (1403 cm^{-1}) in the GO samples [29]. The peak found at 1620 cm^{-1} is a resonance peak that can be assigned to the C–C stretching and absorbed hydroxyl groups in the GO [18]. We also measured the XPS spectroscopy of all samples in order to study the different types of functional groups formed in GO with respect to the degree of oxidation.

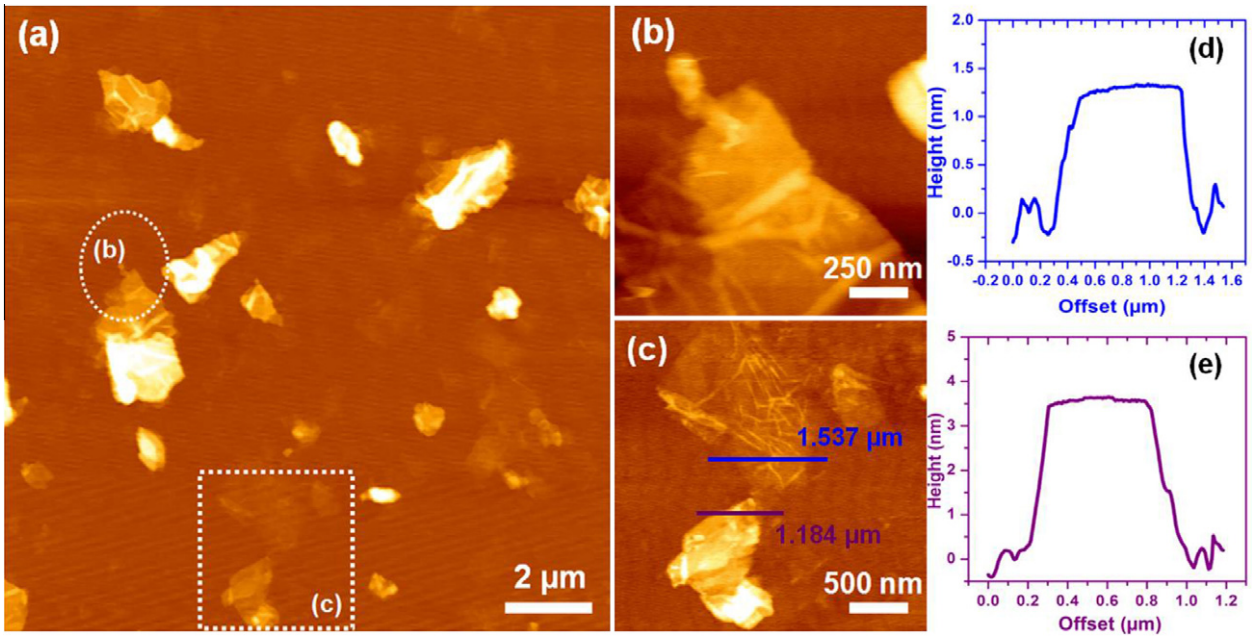

Fig. 4 – (a) Atomic force microscopic image of GO (S-6) nanosheets; (b) enlarged circled area from Fig. 4 (a) and; (c) enlarged squared area from Fig. 4(a). The line profile of the GO nanosheets shown in (c) is represented in (d) and (e).

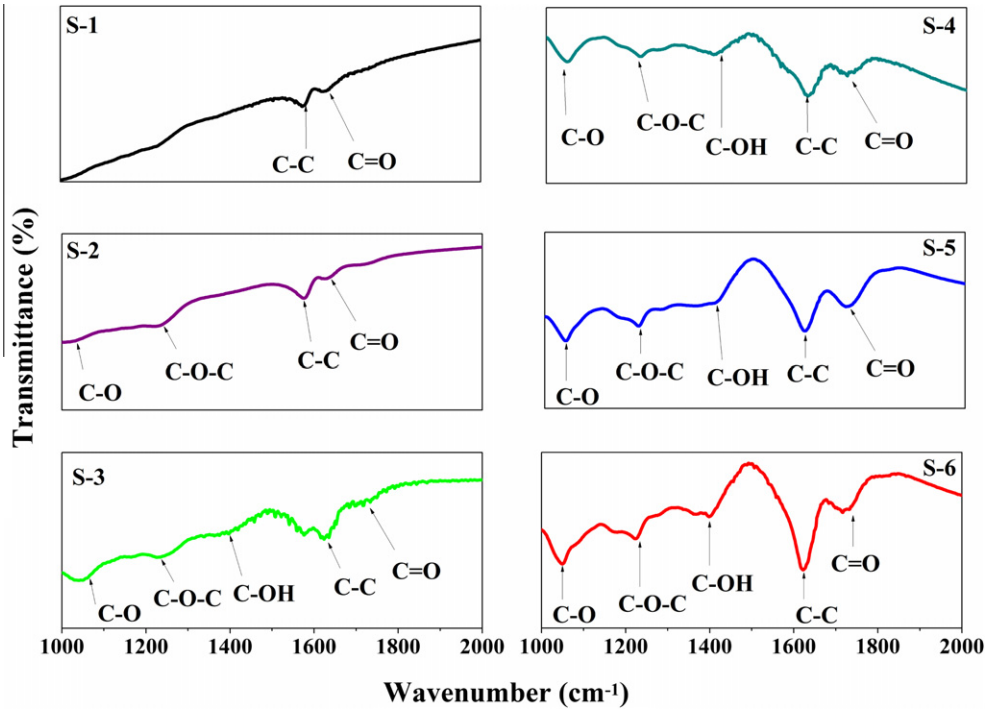

Fig. 5 – Fourier transform infrared spectra of GO with different degrees of oxidation.

3.4. *XPS analysis*

The chemical states of all the samples were investigated by the use of XPS spectra and are shown in Fig. 6. For comparison, the XPS of the pristine graphite was also measured and is shown in the Supplementary document (Fig. S2). In the XPS of graphite, we can see only a peak corresponding to C–C stretching at 284.5 eV indicating the absence of any oxygenated function groups [30]. With increasing the oxidation level, the intensity of the C–C peak due to the sp^2 carbon bond in graphite gradually decreases and an increase in intensity of new functional group's peaks, such as hydroxyl, carboxyl and

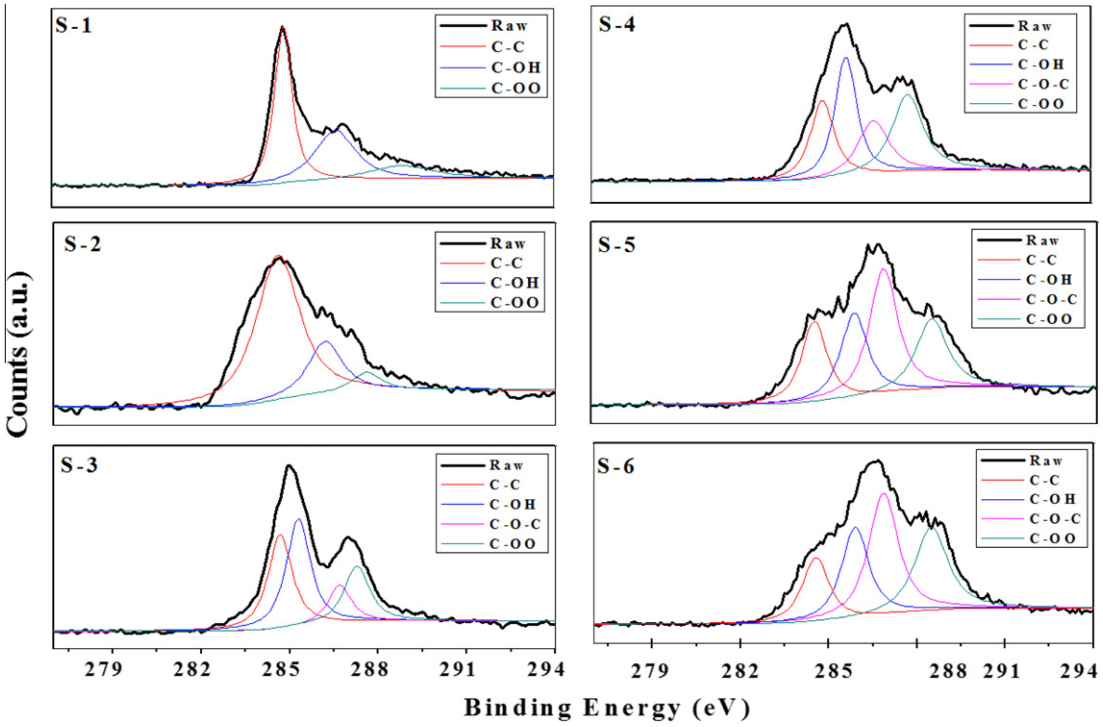

Fig. 6 – X-ray photoelectron spectra of GO with different degrees of oxidation.

epoxyl groups, due to oxidation of graphite are clearly evident from the XPS of the GO at various stages of oxidation. The XPS of sample S-1 shows the presence of C–OH groups in addition to the C–C group in the material and also it possesses a small amount of –O–C=O groups. When the oxidation level is increased, S-2 shows increases in intensity of the C–OH and –O–C=O functional groups and the corresponding intensity of C–C is lower than S-1. Further increases in the oxidation result in the formation of epoxide groups along with the hydroxyl and carboxyl groups, which are clearly noticeable in the XPS of S-3. When the oxidation level is further increased, the XPS of samples S-4, S-5 and S-6 shows that there is an increase in the intensity of epoxide (O–C–O) groups and a decrease in the hydroxyl and carboxyl groups. The sp^2/sp^3 ratio measured from the XPS spectra of samples S-1, S-2, S-3, S-4, S-5, and S-6 are found to be 2.15, 1.52, 0.36, 0.31, 0.27, and 0.25, respectively. The sp^2/sp^3 ratio decreases with increasing oxidation level and is matched well with the previous report in graphite oxide using Staudenmaier process and Brodie method by Lee and Seo [31]. The intensity ratio of the hydroxyl, carboxyl and epoxyl groups with respect to the C-C domains is provided in the Supplementary document (Table S1). This clearly demonstrates that the hydroxyl and carboxyl groups, on further oxidation, lead to the formation of the epoxide groups which results in the increased interlayer spacing in S-6, as seen in the XRD results. The formation of epoxide groups from S-3 level signifies the increase in interlayer spacing and exfoliation of graphitic oxide into GO. This is in agreement with the XRD results of our samples in which S-1 and S-2 samples are graphitic oxide whereas the remaining samples are GO with different oxygen groups.

Hence, the overall analysis of the XPS results demonstrates that the hydroxyl and carboxyl groups are formed at lower oxidation levels and are converted into epoxy groups when the oxidation level is increased. The reason for this complicated mechanism is as follows: the Hummers method employs $KMnO_4$ in conc. H_2SO_4 as the oxidizing agent; this can produce dimanganese heptoxide (Mn_2O_7) which is a strong oxidizer [32]. Mn_2O_7 is capable of epoxidation of unsaturated oxygenated groups [33] formed in the graphite during the oxidation reaction and this results in the higher O–C–O groups in the GO samples with a high oxidation level. To the best of our knowledge no other research group has analyzed the different oxidation levels of GO using Hummers method. The results of the XRD and XPS analysis support the previous finding of Lucas et al. [22].

3.5. *Zeta potential analysis*

The influence of oxygenated functional groups in GO with different degrees of oxidation was evaluated by zeta potential analysis. The zeta potential is a physical property exhibited by any material in dispersion and is an important parameter used for characterizing the electrical properties of interfacial layers in dispersion, which is closely related to the pseudocapacitance behavior of electrode materials used in electrochemical double layer supercapacitors [34]. The zeta potential of all the samples was measured in an aqueous medium and is shown in Fig. 7 as a plot of zeta potential against the different degrees of oxidation. We used the

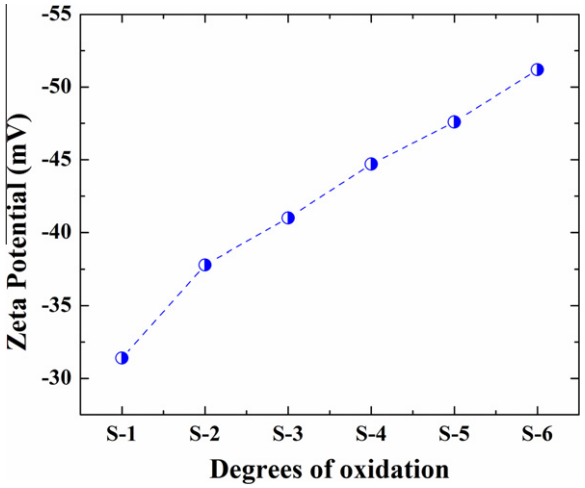

Fig. 7 – Plot of zeta potential vs samples with different oxidation levels.

Smoluchowski approximation [35] for the measurement of the zeta potential of GO. The Smoluchowski expression for plate-like particles [36] is given as $\zeta = \eta\mu/\varepsilon_r\varepsilon_o$, where ζ is the zeta potential, η is the solution viscosity, μ is the electrophoretic mobility and ε is the permittivity of the solution, $\varepsilon = \varepsilon_r\varepsilon_o$.This expression holds good for the zeta potential measurement of lamella type structures like graphene and GO. This finding supports the previous study of Lotya et al. on the zeta analysis of graphene nanosheets [37].

The zeta potential of all the samples is given in the Supplementary document (Fig. S3). The zeta potential measurements show a linear increase in the zeta potential with respect to increasing oxidation levels as seen in Fig. 7. The zeta potential values of S-1, S-2, S-3, S-4, S-5 and S-6 were found to be −31.4, −37.8, −41, −44.7, −47.6, and −51.2 mV, respectively. The negative zeta potential values are due to the presence of electronegative functional groups formed at the graphite lattice during the oxidation [38]. With the successive increase in the oxidation quantity, a greater number of electronegative functional groups are formed in GO resulting in the increase of the zeta potential at higher oxidation levels. Finally, the results for the GO sample S-6 possessing more oxygenated functional groups with a higher zeta potential in an aqueous medium is more likely due to the dissociation of a greater number of acidic groups ($COOH \rightarrow COO^- + H^+$) at the surface thereby resulting in a higher zeta potential. According to the ASTM standard for stability of colloidal suspensions, a zeta potential between 30 and 40 mV (either positive or negative) shows moderate stability, higher than 40 mV (either positive or negative) resembles high stability [39]. Hence, the samples S-1 and S-2 with lower oxidation levels (graphitic oxide) exhibit “moderate stability” whereas the samples with higher oxidation levels (S-3, S-4, S-5 and S-6) exhibit “high stability”.

3.6. *Raman analysis*

Raman spectroscopy is a standard non-destructive tool for the analysis of structural elucidation of carbon materials,

such as graphite, diamond, carbon nanotubes, graphene and GO [40]. Raman spectra were carried out for all the samples with different oxygen contents from S-1 to S6 as shown in Fig. 8. As a reference, the Raman spectrum of precursor graphite was also measured and is shown in the Supplementary document (Fig. S4). The spectrum of graphite shows a strong G band at 1570 cm^{-1} due to first order scattering of the *E2g* mode [41]. It also contains a small band at 1354 cm^{-1} named the *D* band, which is evidence for the presence of defects in the graphite material such as bond-angle disorder, bond-length disorder, vacancies, edge defects, etc., [42] Another important features in the Raman spectra of graphite is the presence of a 2D band at 2700 cm^{-1} (also called the G′ band), this is the overtone of the D band [43]. The 2D band is used to evaluate the structural parameters of the c-axis orientation, since this band is very sensitive to the stacking order of the graphite along the c-axis [44]. It is expected that the harsh chemical oxidation process will result in predominant structural changes in the graphite lattice due to the formation of different types of oxygenated functional groups at the basal plane and also at the edges. Fig. 8 shows the Raman spectra of all the samples and shows significant changes at different degrees of oxidation. In S-1, the G band is shifted towards a higher wavenumber (1585 cm^{-1}) due to the oxidation of graphite and the D band has a higher intensity, which can attributed to the formation of defects and disorder such as the presence of *in-plane* hetero-atoms, grain boundaries, aliphatic chain, etc., On the other hand, the intensity of the 2D band is smaller after oxidation, a new band appeared around 2950 cm^{-1} which is denoted as D + G band. The decrease in the 2D band is due to the breaking of the stacking order due to the oxidation reaction.

Fig. 9a shows the corresponding changes in the G band with respect to levels of oxidation. It shows that the G band is shifted towards a higher wavenumber with the increase in oxidation level. At the highest oxidation level, the G band position reaches a position at 1596 cm^{-1}. The shift in G band is associated with the formation of new sp^3 carbon atoms in the graphite lattice [45]. In addition to the shift in G band position; the full width half maximum (FWHM) of the G band also increases with respect to the oxidation level. The FWHM of the G band with increasing oxidation level was 45, 54, 70, 103, 114, and 124 cm^{-1}, for the samples S-1, S-2, S-3, S-4, S-5, and S-6, respectively. The shift in G band increase in FWHM suggests that the presence of sp^3 carbons is increased with respect to oxidation level. Similarly, the different degrees of oxidation affect the nature of D band. The intensity of the D band increases with increasing oxidation and becomes constant at higher oxidation levels. The FWHM of the D band linearly increase with the increase in oxidation levels indicating that the oxidation process highly influences the *in-plane* sp^2 domains of the graphite with defects [45]. Fig. 9b shows the variation of $I_{(D)}/I_{(G)}$ with respect to the oxidation level. It shows that lower oxidation levels result in an increase in the $I_{(D)}/I_{(G)}$ ratio, which decreases with increasing oxidation, and finally becomes saturated at higher oxidation levels. The decrease in $I_{(D)}/I_{(G)}$ ratio at higher levels of oxidation is compensated by the increase in the FWHM of the G band.

The peaks correspond to overtones, such as the 2D, D + G and 2G bands, which also display significant changes depending on the oxidation. The intensity of the 2D band decreases

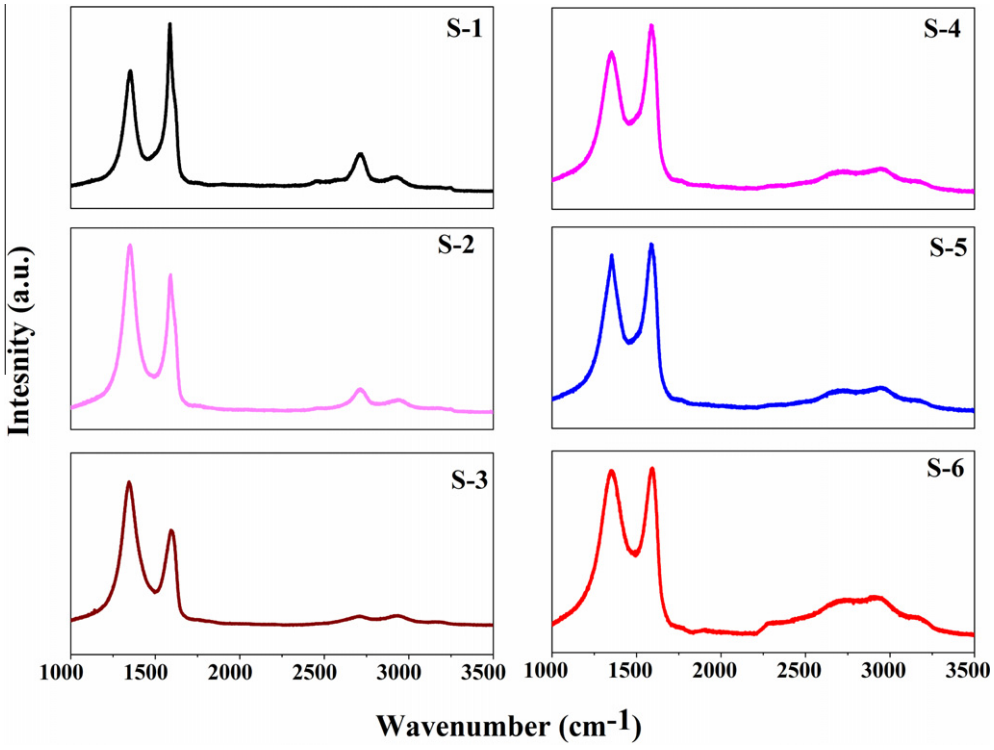

Fig. 8 – Raman spectroscopy of GO with different degrees of oxidation.

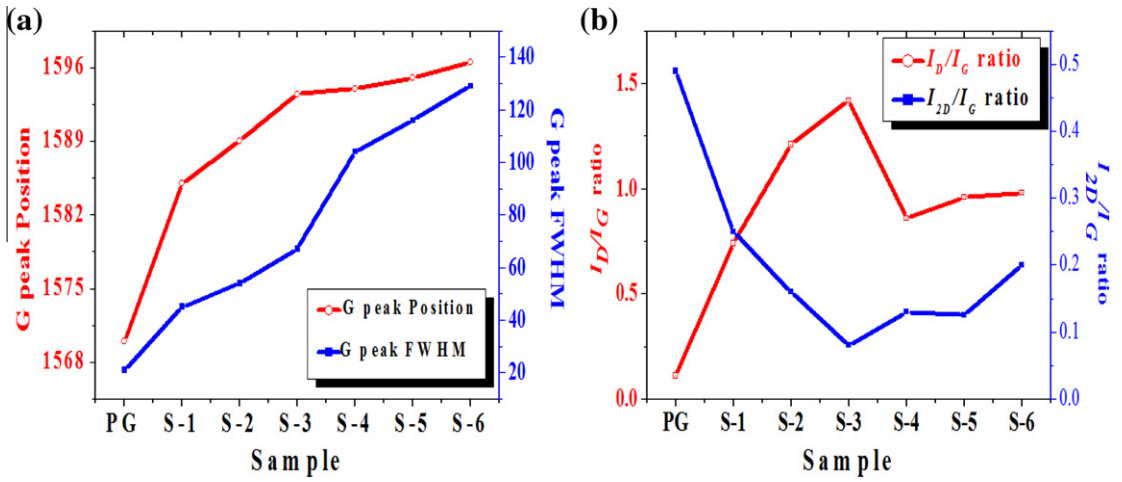

Fig. 9 – (a) Dependence of G band position and FWHM with respect to oxidation level. (b) Variation of $I_{(D)}/I_{(G)}$ ratio and $I_{(2D)}/I_{(G)}$ ratio with respect to oxidation level. PG refers to pristine graphite.

with increases in oxidation level and broadens at the higher oxidation levels. Fig. 9b represents the change in $I_{(2D)}/I_{(G)}$ ratio with respect to oxidation level. It decreases up to S-3 and then increases oxidation levels higher than S-3. Since the 2D band is structure sensitive [44], the $I_{(2D)}/I_{(G)}$ ratio clearly illustrates the transition from crystalline to an amorphous phase in GO upon oxidation. Similarly, the other overtone bands D + G (2922 cm^{-1}) and 2G (3171 cm^{-1}) increased with increasing oxidation level. The changes in overtone bands, such as 2D, D + G and 2G bands, illustrate the disruption of the graphitic *AB* stacking order in GO with increasing oxidation level. The average crystallite size of the sp^2 domains in the GO samples can be calculated by the intensity measures of the D band ($I_{(D)}$) and G band ($I_{(G)}$) [45,46]. Many equations such as Tuinstra and Koenig's equation [41], the Knight and White relation [47], have been employed to measure the average crystallite size of the sp^2 domains using the $I_{(D)}/I_{(G)}$ ratio. Later on, the general equation of the average crystallite size of the sp^2 domains L_a in the nanographite sytems was given by Cancodo et al. [48] by relating the $I_{(D)}/I_{(G)}$ ratio to the fourth power of the laser energy used in the experiment. This modified equation can be given as.

$$L_a(\mathrm{nm}) = [(2.4 * 10^{-10})(\lambda_l)^4]/[I_{(D)}/I_{(G)}] \quad (1)$$

where L_a is the average crystallite size of the sp^2 domains, λ_l is the input laser energy, $I_{(D)}$ is the intensity of the D band, and $I_{(G)}$ is the intensity of the G band. The calculated L_a values are 18.24, 11.25, 9.63, 15.67, 14.06, and 13.77 nm, for samples S-1, S-2, S-3, S-4, S-5 and S-6, respectively. The L_a value of the precursor graphite was calculated to be 122 nm. The results indicate that the average crystallite size decreases with less oxidation; this may be due to the breaking of crystallites with initial oxidation resulting in the formation of defects, disorders, sp^3 hybridization and changes in crystallinity. At the same time, L_a starts increasing for sample S-4 and becomes constant (around 14 nm for S-5 and S-6) at higher levels of oxidation. This is in agreement with the previous investigations on the crystallite size of series of graphite oxide using Staudenmaier method as evaluated by Lucas et al. [22]. The recent investigation on the oxidation of mechanically exfoliated graphene by Wang et al. also supports our findings [49]. In these aspects, there is no straightforward relation between the oxidized (sp^3) and unoxidized (sp^2) states with respect to level of oxidation. Overall, the Raman spectroscopy results show the transition of crystalline graphite into an amorphous state and the disruption of stacking order with respect to increases in the oxidation level. However, there are much further investigations needed to study the detailed physics and chemistry underlying the structure of GO.

3.7. *Electrochemical properties*

The influence of oxygenated functional groups in GO was also studied by using CV measurements using a 5 mM solution of potassium ferricyanide $[K_3(FeCN)_6]$ containing 0.1 M KCl solution. The oxygenated functional groups present in GO nanosheets play a key role in electrochemical biosensors for glucose sensing, supercapacitors, etc., [50]. Hence a study on the electrochemical properties of GO with different oxidation level is an area of potential interest. Herein, the GO sample is modified onto the surface of a GCE electrode. Fig. 10 shows the CV curves of all the tested samples in comparison with the GCE electrode. It shows that the typical redox reaction occurred at the electrode surface indicating the presence of an anodic peak and cathodic peak in the CV curves. It is clear from Fig. 10a, that samples S-1 and S-2 show a higher current value for the redox reaction than the GCE electrode. As evident from the XPS and zeta potential measurement stated above, these samples contain less oxygenated functional groups, thereby less surface charge which enables them to attract ferricyanide ions to the electrode surface for the electrochemical reaction. Similarly, the samples S-3 and S-4 show higher electrochemical reactions compared with the GCE (as shown in Fig. 10b) but lower than the samples S-1 and S-2. This is due to the increase in surface oxygen groups and surface charge. Fig. 10c displays the CV curves of samples S-5 and S-6 and shows a significant reduction in the cathodic peak current (I_{pc}) compared with the GCE and is due to the

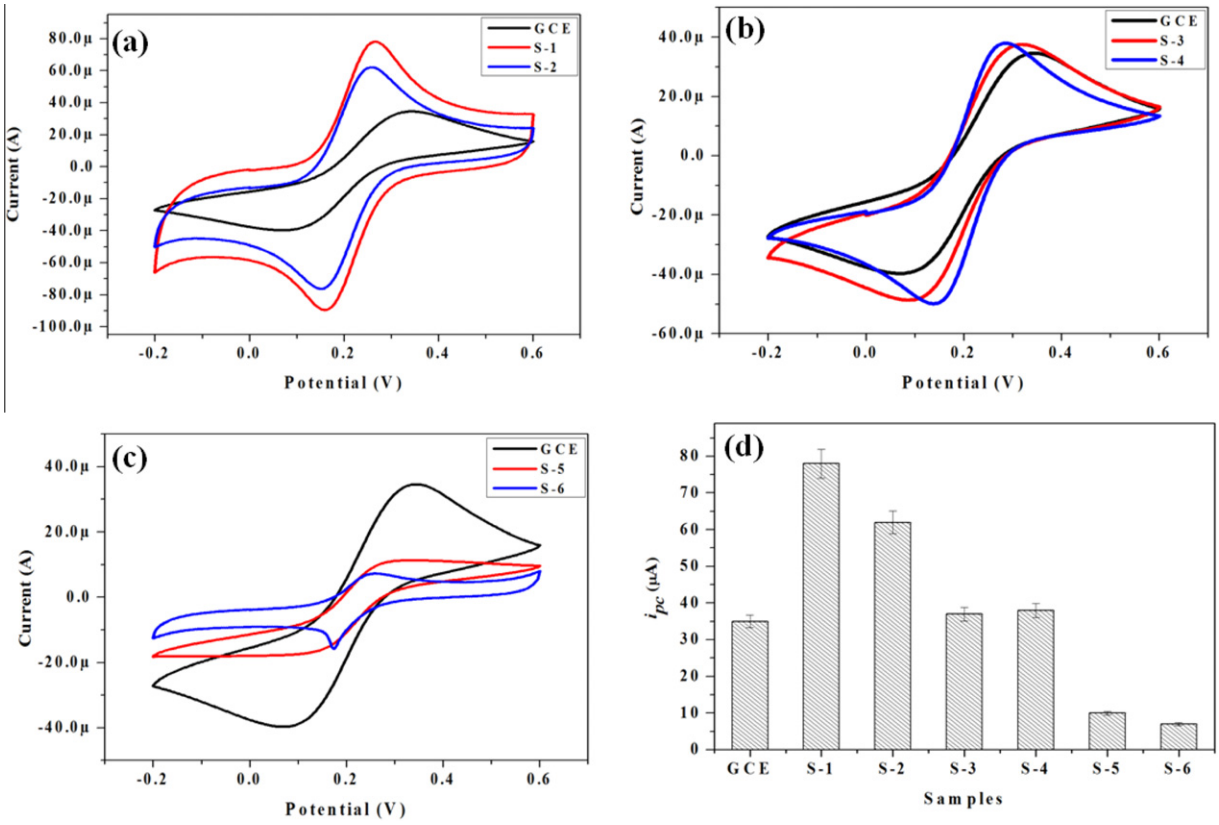

Fig. 10 – (a-c) Cyclic voltammetry of GO samples (S-1 to S-6) modified on GCE electrodes in 5 mM $K_3[Fe(CN)_6]$ containing 0.1 M KCl solution. (d) Comparison of I_{pc} of the samples with different oxidation levels.

high surface charge of these samples (as evident from the XPS and zeta potential measurements). Both S-5 and S-6 with higher levels of oxidation act as an insulating layer on the GCE electrode and due to their high surface charge, the ferricyanide ions are repelled at the electrode surface thereby limiting electrochemical reactions. The electrochemical behavior of the S-6 sample is consistent with the previous studies of Guo et al. [51]. However, it is still remaining elusive to determine the contribution of each functional group on the electrochemical properties of GO due to its structural and chemical inhomogeneous nature. The histogram curve of all the samples in comparison with the GCE electrode is shown in Fig. 10(d). It shows that the I_{pc} value decreases with increasing levels of oxidation, thereby showing the transition from metallic to semiconducting and insulating behavior due to increases in oxidation level.

4. Summary

We synthesized GO using a modified Hummers method with different degrees of oxidation. The formation of various oxygenated functional groups at different stages of oxidation and their influence on the chemical and structural analysis was investigated. The XRD studies revealed that the graphitic nature of the material decreased with increasing oxidation level. The morphological studies using TEM showed a sheet like morphology in all stages of oxidation. XPS analyses showed the formation of hydroxyl and carboxyl groups in the graphite lattice during the initial stage of oxidation and these were converted into epoxide groups at higher oxidation levels. The various degrees of oxidation significantly altered the zeta potential properties exhibiting moderate stability at lower oxidation levels and high stability at higher oxidation levels. Moreover, a detailed study on the Raman spectra at various levels of the oxidized samples was presented. It showed that the sp^3 domains are increasing with increase in oxidation level with the disruption of the graphitic stacking order. The influence of oxygenated functional groups in different GO significantly altered the electrochemical properties of GO. The key findings of our work support the view of the tunable properties of GO, that is, by varying the oxidization degree which can provide new positive features in the development of GO-based device applications.

Acknowledgement

This research was supported by a National Research Foundation of Korea Grant under contract number 2011-0015829.

Appendix A. Supplementary data

Supplementary data associated with this article can be found, in the online version, at http://dx.doi.org/10.1016/j.carbon.2012.10.013.

REFERENCES

[1] Dikin DA, Stankovich S, Zimney EJ, Piner RD, Dommett GHB, Evmenenko G, et al. Preparation and characterization of graphene oxide paper. Nature 2007;448:457–60.
[2] Long D, Li W, Ling L, Miyawaki J, Mochida I, Yoon S-H. Preparation of nitrogen-doped graphene sheets by a combined chemical and hydrothermal reduction of graphene oxide. Langmuir 2010;26:16096–102.
[3] Dreyer DR, Park S, Bielawski CW, Ruoff RS. The chemistry of graphene oxide. Chem Soc Rev 2010;39:228–40.
[4] Kim J, Cote LJ, Kim F, Yuan W, Shull KR, Huang J. Graphene oxide sheets at interfaces. J Am Chem Soc 2010;132:8180–6.
[5] Wang G, Wang B, Park J, Yang J, Shen X, Yao J. Synthesis of enhanced hydrophilic and hydrophobic graphene oxide nanosheets by a solvothermal method. Carbon 2009;47:68–72.
[6] Brodie BC. On the atomic weight of graphite. Philos Trans R Soc London 1859;149:249–59.
[7] Park S, Ruoff RS. Chemical method for production of graphenes. Nat Nanotechnol 2009;4:217–24.
[8] Wang G, Sun X, Li C, Lian J. Tailoring oxidation degrees of graphene oxide by simple chemical reactions. Appl Phys Lett 2011;99(053114):1–3.
[9] Krishnamoorthy K, Mohan R, Kim S-J. Graphene oxide as a photocatalytic material. Appl Phys Lett 2011;98(244101):1–3.
[10] Khan U, May P, Neill AO, Coleman JN. Development of stiff, strong, yet tough composites by the addition of solvent exfoliated graphene to polyurethane. Carbon 2010;48:4035–41.
[11] Cheng Q, Tang J, Ma J, Zhang H, Shinya N, Qin L-C. Graphene and nanostructured MnO_2 composite electrodes for supercapacitors. Carbon 2011;49:2917–25.
[12] Loh KP, Bao Q, Eda G, Chhowalla M. Graphene oxide as a chemically tunable platform for optical applications. Nat Chem 2010;2:1015–24.
[13] Jeong HK, Yang C, Kim BS, Kim K. Valence band of graphite oxide. Europhys Lett 2010;92(37005):1–4.
[14] Shukla S, Saxena S. Spectroscopic investigation of confinement effects on optical properties of graphene oxide. Appl Phys Lett 2011;98(073104):1–3.
[15] Veerapandian M, Lee M-H, Krishnamoorthy K, Yun K. Synthesis, characterization and electrochemical properties of functionalized graphene oxide. Carbon 2012;50:4228–38.
[16] Staudenmaier L. Method for the preparation of graphitic acid. Ber Dtsch Chem Ges 1898;31:1481–7.
[17] Hummers WS, Offeman RE. Preparation of graphitic oxide. J Am Chem Soc 1958;80:1339–49.
[18] Gunasekaran V, Krishnamoorthy K, Mohan R, Kim S-J. An investigation of the electrical transport properties of graphene-oxide thin films. Mater Chem Phys 2012;132:29–33.
[19] Jeong HK, Jin MH, So KP, Lim SC, Lee YH. Tailoring the characteristics of graphite oxides by different oxidation times. J Phys D Appl Phys 2009;42(065418):1–6.
[20] Jeong H-K, Lee YP, Lahaye RJWE, Park M-H, An KH, Kim I-J, et al. Evidence of graphitic AB stacking order of graphite oxides. J Am Chem Soc 2008;130:1362–6.
[21] Marcano DC, Kosynkin DV, Berlin JM, Sinitskii A, Sun Z, Slesarev A, et al. Improved synthesis of graphene oxide. ACS Nano 2010;4:4806–14.
[22] Lucas CH, Peinado AJL, Gonzalez DL, Cervantes MLR, Aranda RMM. Study on oxygen-containing groups in a series of graphite oxides: physical and chemical characterization. Carbon 1995;33:1585–92.
[23] Wilson NR, Pandey PA, Beanland R, Young RJ, Kinloch IA, Gong L, et al. Graphene oxide: structural analysis and application as a highly transparent support for electron microscopy. ACS Nano 2009;3:2547–56.
[24] Cruz FA, Cowley JM. Structure of graphitic oxide. Nature 1962;196:468–9.
[25] Cruz FA, Cowley JM. An electron diffraction study of graphitic oxide. Acta Crystallogr 1963;16:531–4.
[26] Shukla S, Saxena S. Spectroscopic investigation of confinement effects on optical properties of graphene oxide. Appl Phys Lett 2011;98(073104):1–3.
[27] Bonaccorso F, Sun Z, Hasan T, Ferrari AC. Graphene photonics and optoelectronics. Nat Photonics 2010;4:611–22.
[28] Krishnamoorthy K, Veerapandian M, Mohan R, Kim S-J. Investigation of Raman and photoluminescence studies of reduced graphene oxide sheets. Appl Phys A 2012;106:501–6.
[29] Krishnamoorthy K, Navaneethaiyer U, Mohan R, Lee J, Kim S-J. Graphene oxide nanostructures modified multifunctional cotton fabrics. Appl Nanosci 2012;2:119–26.
[30] Zhao G, Shao D, Chen C, Wang X. Synthesis of few-layered graphene by H_2O_2 plasma etching of graphite. Appl Phys Lett 2011;98(183114):1–3.
[31] Lee DW, Seo JW. Sp^2/sp^3 carbon ratio in graphite oxide with different preparation times. J Phys Chem C 2011;115:2705–8.
[32] Dash S, Patel S, Mishra BK. Oxidation by permanganate: synthetic and mechanistic aspects. Tetrahedron 2009;65:707–39.
[33] Tromel M, Russ M. Dimanganese heptoxide for the selective oxidation of organic substrates. Angew Chem Int Ed Engl 1987;26:1007–9.
[34] Kim TY, Lee HW, Stoller M, Dreyer DR, Bielawski CW, Ruoff RS, et al. High-performance supercapacitors based on poly(ionic liquid)-modified graphene electrodes. ACS Nano 2011;5:436–42.
[35] Dukhin AS, Goetz PJ. Ultrasound for characterizing colloids: particle sizing, zeta potential and rheology. Elsevier; 2002.
[36] Ohshima H. Theory of colloid and interfacial electric phenomena. New York: Elsevier; 2006.
[37] Lotya M, Hernandez Y, King PJ, Smith RJ, Nicolosi V, Karlsson LS, et al. Liquid phase production of graphene by exfoliation of graphite in surfactant/water solutions. J Am Chem Soc 2009;131:3611–20.
[38] Jung I, Dikin DA, Piner RD, Ruoff RS. Tunable electrical conductivity of individual graphene oxide sheets reduced at "low" temperatures. Nano Lett 2008;8:4283–7.
[39] ASTM, Zeta potential of colloids in water and waste water. ASTM Standard D 4187–82. American Society for Testing and Materials; 1985.
[40] Livneh T, Haslett TL, Moskovits M. Distinguishing disorder-induced bands from allowed Raman bands in graphite. Phys Rev B 2002;66(195110):1–11.
[41] Tuinstra F, Koenig JL. Raman spectrum of graphite. J Chem Phys 1970;53:1126–30.
[42] Venugopal G, Jung M-H, Suemitsu M, Kim S-J. Fabrication of nanoscale three-dimensional graphite stacked junctions by focused-ion-beam and observation of anomalous transport characteristics. Carbon 2011;49:2766–72.
[43] Vasu KS, Chakraborty B, Sampath S, Sood AK. Probing top-gated field effect transistor of reduced graphene oxide monolayer made by dielectrophoresis. Solid State Comm 2010;150:1295–8.
[44] Pimenta MA, Dresselhaus G, Dresselhaus MS, Cancado LG, Jorio A, Saitoe R. Studying disorder in graphite-based systems by Raman spectroscopy. Phys Chem Chem Phys 2007;9:1276–91.
[45] Ferrari AC, Robertson J. Interpretation of Raman spectra of disordered and amorphous carbon. Phys Rev B 2000;61:14095–107.
[46] Krishnamoorthy K, Veerapandian M, Zhang LH, Yun KS, Kim SJ. Antibacterial efficiency of graphene nanosheets against pathogenic bacteria via lipid peroxidation. J Phys Chem C 2012;116:17280–7.

[47] Knight DS, White W. Characterization of diamond films by Raman spectroscopy. J Mater Res 1989;4:385–93.
[48] Cancado LG, Takai K, Enoki T, Endo M, Kim YA, Mizusaki H, et al. General equation for the determination of the crystallite size La of nanographite by Raman spectroscopy. Appl Phys Lett 2006;88(163106):1–3.
[49] Wang S, Wang R, Liu X, Wang X, Zhang D, Guo Y, et al. Optical spectroscopy investigation of the structural and electrical evolution of controllably oxidized graphene by a solution method. J Phys Chem C 2012;116:10702–7.
[50] Xu B, Yue S, Sui Z, Zhang X, Hou S, Cao G, et al. What is the choice for supercapacitors: graphene or graphene oxide? Energy Environ Sci 2011;4:2826–30.
[51] Guo H-L, Wang X-F, Qian Q-Y, Wang F-B, Xia X-H. A green approach to the synthesis of graphene nanosheets. ACS Nano 2009;3:2653–9.